

# GRB 140515A AT $z=6.33$ : CONSTRAINTS ON THE END OF REIONIZATION FROM A GAMMA-RAY BURST IN A LOW HYDROGEN COLUMN DENSITY ENVIRONMENT

RYAN CHORNOCK<sup>1</sup>, EDO BERGER<sup>1</sup>, DEREK B. FOX<sup>2,3</sup>, WEN-FAI FONG<sup>1</sup>, TANMOY LASKAR<sup>1</sup>, AND KATHERINE C. ROTH<sup>4</sup>

*Draft version May 30, 2014*

## ABSTRACT

We present the discovery and subsequent spectroscopy with Gemini-North of the optical afterglow of the *Swift* gamma-ray burst (GRB) 140515A. The spectrum exhibits a well-detected continuum at wavelengths longer than 8915 Å with a steep decrement to zero flux blueward of 8910 Å due to Ly $\alpha$  absorption at redshift  $z \approx 6.33$ . Some transmission through the Ly $\alpha$  forest is present at  $5.2 < z < 5.733$ , but none is detected at higher redshift, consistent with previous measurements from quasars and GRB 130606A. We model the red damping wing of Ly $\alpha$  in three ways that provide equally good fits to the data: (a) a single host galaxy absorber at  $z = 6.327$  with  $\log(N_{\text{HI}}, \text{cm}^{-2}) = 18.62 \pm 0.08$ ; (b) pure intergalactic medium (IGM) absorption from  $z = 6.0$  to  $z = 6.328$  with a constant neutral hydrogen fraction of  $\bar{x}_{\text{HI}} = 0.056_{-0.027}^{+0.011}$ ; and (c) a hybrid model with a host absorber located within an ionized bubble of radius 10 comoving Mpc in an IGM with  $\bar{x}_{\text{HI}} = 0.12 \pm 0.05$  ( $\bar{x}_{\text{HI}} \lesssim 0.21$  at the  $2\sigma$  level). Regardless of the model, the sharpness of the dropoff in transmission is inconsistent with a substantial neutral fraction in the IGM at this redshift. No narrow absorption lines from the host galaxy are detected, indicating a host metallicity of  $[Z/H] \lesssim -0.8$ . Even if we assume that all of the hydrogen absorption is due to the host galaxy, the column is unusually low for a GRB sightline, similar to two out of the other three highest-redshift bursts with measured  $\log(N_{\text{HI}})$ . This is possible evidence that the escape fraction of ionizing photons from normal star-forming galaxies increases at  $z \gtrsim 6$ .

*Subject headings:* gamma-ray burst: individual (GRB 140515A) — intergalactic medium — dark ages, reionization, first stars

## 1. INTRODUCTION

The reionization of the intergalactic medium (IGM) by the first stars and quasars was likely a complex process. Current evidence from observations of polarization of the cosmic microwave background implies a redshift for reionization of  $z \approx 10$  (Hinshaw et al. 2013), while tracers at lower redshift suggest that the tail end of the process was still ongoing at redshifts  $z \approx 6$  (Fan et al. 2006a). Gamma-ray bursts (GRBs) offer one of the most promising probes of this epoch due to their bright afterglows, which can be seen at cosmological distances and lack some of the complications of quasar observations (e.g., Lamb & Reichart 2000; Barkana & Loeb 2004).

In this *Letter*, we present our Gemini spectrum of the afterglow of the long-duration GRB 140515A. It reveals a sharp decrement in flux shortward of  $\sim 8900$  Å, implying a redshift of  $z \approx 6.32$  (Chornock et al. 2014a), which we refine below. This makes GRB 140515A the burst with the third largest spectroscopic redshift. Only GRBs 080913 ( $z=6.733$ ; Greiner et al. 2009; Patel et al. 2010) and 090423 ( $z \approx 8.23$ ; Tanvir et al. 2009; Salvaterra et al. 2009) are known to be more distant, although GRB 090429B has a photometric redshift

of  $\sim 9.4$  (Cucchiara et al. 2011). It is important to note that at the time of our Gemini observations, no optical observations or photometric redshift estimates had been reported in the GCN Circulars, so the high- $z$  nature of the burst was purely serendipitous.

We describe our spectroscopic observations in Section 2 and analyze the spectrum to set constraints on the opacity of the IGM at  $z > 5.2$  in section 3. We fit the red damping wing of Ly $\alpha$  with three fiducial models in Section 4 to set limits on the neutral fraction of the IGM. We conclude in Section 5 by placing these observations in the context of other constraints on reionization.

## 2. OBSERVATIONS

GRB 140515A was detected by *Swift* at 09:12:36 UT on 2014 May 15 (D’Avanzo et al. 2014). We initiated followup observations with the Gemini Multi-Object Spectrograph (GMOS; Hook et al. 2004) on the 8 m Gemini-North telescope at 10:48 UT and discovered a faint optical source consistent with the X-ray afterglow position (D’Avanzo et al. 2014) in our  $i$  and  $z$  acquisition images (Fong et al. 2014). We obtained a dithered pair of 900 s spectra starting at 11:42 UT on 2015 May 15 (2.5 hr after the BAT trigger; D’Avanzo et al. 2014). During the observations, the source position increased in airmass from 2.38 to 3.00. We oriented the 1''-wide slit at a position angle of  $78^\circ 3'$ , which was within  $5^\circ$  of the parallactic angle, so differential slit losses should be minimal. We used the R400 grating with an OG515 filter to cover the wavelength range 5888–10162 Å. The GMOS focal plane has three abutting CCDs and we were only able to obtain observations with a single grating angle, so our

<sup>1</sup> Harvard-Smithsonian Center for Astrophysics, 60 Garden Street, Cambridge, MA 02138, USA; rchornock@cfa.harvard.edu

<sup>2</sup> Department of Astronomy and Astrophysics, Pennsylvania State University, 525 Davey Laboratory, University Park, PA 16802, USA

<sup>3</sup> Sabbatical address: Max Planck Institute for Extraterrestrial Physics, Giessenbachstrasse, 85741 Garching, Germany

<sup>4</sup> Gemini Observatory, 670 North Aohoku Place, Hilo, HI 96720, USA

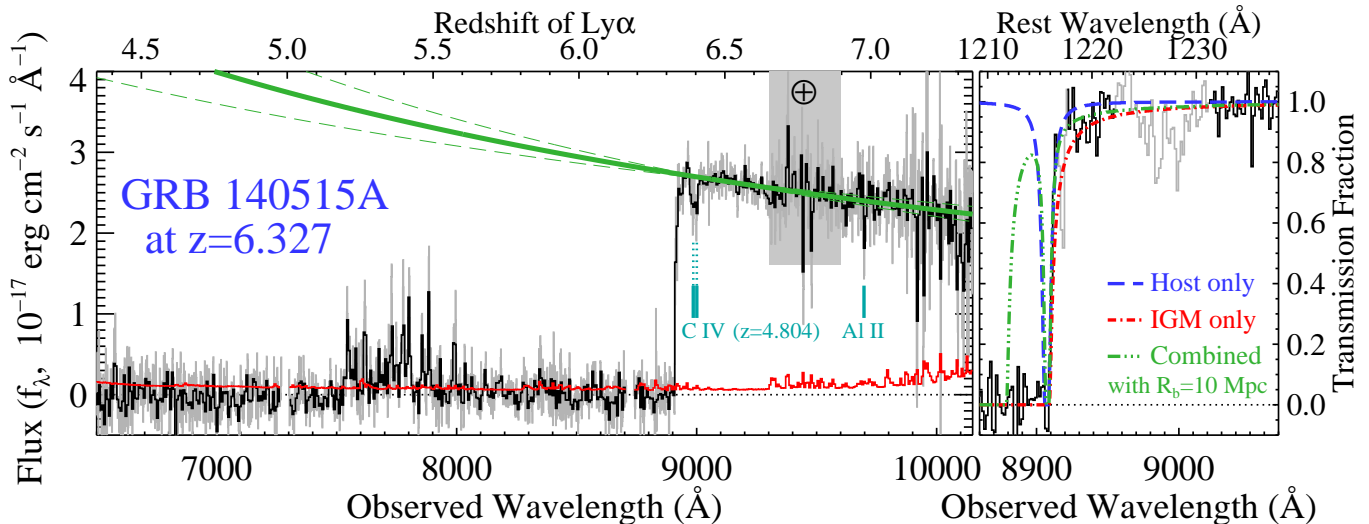


**Figure 1.** *Left:* GMOS spectrum of the optical afterglow of GRB 140515A. The gray spectrum is unbinned, while the black version has been binned by 5 pixels. The red line is the  $1\sigma$  uncertainty of the binned spectrum. The solid green line is a power-law fit to the afterglow continuum and the dashed green lines represent power laws with slopes of  $\pm 3\sigma$ . The gray box with the  $\oplus$  symbol marks the region possibly containing residuals from the correction for telluric  $\text{H}_2\text{O}$  absorption. Absorption lines from a foreground absorber are marked in cyan. *Right:* Zoomed-in view of the normalized unbinned spectrum near  $\text{Ly}\alpha$ . The three lines represent three fits to the red damping wing of the  $\text{Ly}\alpha$  profile with  $z_{\text{GRB}}$  allowed to vary (blue: absorber at the host redshift only; red: no host contribution, but a uniform IGM with a constant ionization fraction at  $6.0 < z < z_{\text{GRB}}$ ; green: a combined model where the GRB host resides inside an ionized bubble with a radius of 10 comoving Mpc). The rest wavelength scale at the top assumes the value derived from the host-only fit of  $z=6.327$ . The spectral bins in light gray were excluded from the fit. See text for details.

data have two gaps at 7275–7298 Å and 8709–8737 Å. In addition to the high airmass, the moon was >99% illuminated, so the sky background was extremely high. Fortunately, the seeing was exceptional, with a full-width at half-maximum (FWHM) of  $0''.45$  in the acquisition images (Fong et al. 2014) and even in our final spectrum, the spatial FWHM of the object trace was only  $0''.6$ . The spectral FWHM of night sky emission lines are  $\sim 7$  Å, but due to the excellent seeing, the object did not fill the slit and the resolution of the object spectrum is  $\sim 5$  Å.

We use IRAF<sup>5</sup> to perform basic two-dimensional image processing, remove cosmic rays (van Dokkum 2001), and shift and stack the two-dimensional frames prior to spectral extraction. We apply flux calibrations and correct for telluric absorption using our own IDL procedures and archival observations of standard stars taken with a similar setup. The airmass of our data was substantially higher than any suitable standard star observations that we are able to locate in the Gemini archive, so the overall spectral shape of the final spectrum is somewhat uncertain, although this does not affect any of our analysis. In addition, we are careful to manually scale the correction for telluric  $\text{H}_2\text{O}$  absorption near 9400 Å because of the large airmass difference with the available standards. We also correct the spectrum for  $E(B - V) = 0.02$  mag of Galactic extinction (Schlafly & Finkbeiner 2011).

The final extracted spectrum is shown in Figure 1. The sharp decrement in flux shortward of 8910 Å is evidence of  $\text{Ly}\alpha$  absorption at  $z \approx 6.33$ . We fit a power law to the continuum flux at 9020–9870 Å, while excluding the region of the most uncertain telluric correction near 9400 Å and find a best fit of  $f_\lambda \propto \lambda^{-1.56 \pm 0.13}$ , which is shown as

the solid green line. The value for the slope has additional uncertainty due to low-level telluric absorption over most of the available continuum.

We search the afterglow continuum for narrow absorption features from the host galaxy interstellar medium but find no plausible matches at wavelengths compatible with the approximate redshift of  $\text{Ly}\alpha$ , so we are unable to make a precise measurement of the redshift of GRB 140515A ( $z_{\text{GRB}}$ ), a point that we will return to below. Instead, we find unresolved absorption lines at 8985.2, 9000.0, and 9697.9 Å that are consistent with the C IV  $\lambda\lambda$  1548, 1551 doublet and Al II  $\lambda$ 1670 from an intervening absorber at  $z = 4.804$ . A possible weak absorption feature at 9170.4 Å, with an observed-frame equivalent width ( $EW$ ) of  $2.1 \pm 0.8$  Å, does not match any other expected line from the absorber or the host galaxy<sup>6</sup>.

### 3. IGM OPACITY

We first examine the transparency of the IGM to  $\text{Ly}\alpha$  photons over the redshift range  $5.2 < z < 6.3$ . The signal-to-noise ratio (S/N) of these data (peaking in the continuum at  $\sim 20$  per  $1.38$  Å pixel near 9000 Å) are not as high as for GRB 130606A (Chornock et al. 2013) or for typical high- $z$  quasar observations but still place meaningful constraints. We inspect the sky-subtracted two-dimensional spectra and find no clear transmitted continuum over the wavelength range 8185–8905 Å (corresponding to redshifts of 5.733–6.325 relative to  $\text{Ly}\alpha$ ).

We follow Fan et al. (2006b) and define an effective optical depth to  $\text{Ly}\alpha$ ,  $\tau_{\text{GP}}^{\text{eff}} = -\ln(\mathcal{T})$ , where  $\mathcal{T}$  is the

<sup>6</sup> We note that a foreground galaxy fell in our spectroscopic slit  $\sim 3''.5$  away from the GRB afterglow. It exhibits a single spectrally-resolved emission line at 8200 Å, which we identify as [O II]  $\lambda$ 3727 at  $z=1.200$ . No strong absorption lines from that galaxy are expected in our limited continuum wavelength interval.

<sup>5</sup> IRAF is distributed by the National Optical Astronomy Observatories, which are operated by the Association of Universities for Research in Astronomy, Inc., under cooperative agreement with the National Science Foundation.

**Table 1**  
GRB 140515A Ly $\alpha$  Transmission

Redshift Range	Line	Transmission	$\tau_{\text{GP}}^{\text{eff}}(\text{Ly}\alpha)$
5.20–5.26 <sup>a</sup>	Ly $\alpha$	0.082	2.51
5.26–5.41	Ly $\alpha$	0.094	2.37
5.41–5.56	Ly $\alpha$	0.062	2.78
5.56–5.71	Ly $\alpha$	0.029	3.53
5.71–5.86	Ly $\alpha$	<0.014 <sup>c</sup>	>4.3
5.86–6.01	Ly $\alpha$	<0.019	>4.0
6.01–6.16	Ly $\alpha$	<0.016	>4.2
6.19–6.31	Ly $\alpha$	<0.022	>3.8
5.96–6.08 <sup>b</sup>	Ly $\beta$	<0.103	>5.1
6.15–6.30	Ly $\beta$	<0.117	>4.8

<sup>a</sup> Lower redshift limit truncated to avoid Ly $\beta$  absorption from host

<sup>b</sup> Redshift limits set to avoid Ly $\gamma$  and a CCD chip gap

<sup>c</sup> Upper limits are  $3\sigma$

average transmission relative to the continuum in a bin. To compare to previously reported results from  $z \approx 6$  quasars and GRB 130606A, we compute  $\tau_{\text{GP}}^{\text{eff}}$  in bins of width  $\Delta z = 0.15$ , taking care to define our wavelength intervals to avoid Ly $\beta$  and the CCD gaps. We also measure the transmission in the Ly $\beta$  forest and convert these to effective Ly $\alpha$  opacities using the same correction factors as Fan et al. (2006b). We present the results in Figure 2 along with the numerical values in Table 1. We do not detect any transmission at  $z > 5.71$ , but we are able to set lower limits on  $\tau_{\text{GP}}^{\text{eff}}$  of  $\sim 4$ . Collectively, the results from the two GRB sightlines are generally consistent with those seen towards quasars.

The large redshift bins used above effectively overweight the transmission to regions of lower opacity and are a crude tracer of Ly $\alpha$  opacity when the optical depth is large. Instead, higher-order statistics, such as the distribution of length scales of dark gaps (e.g., Songaila & Cowie 2002) or pixel-scale transmission statistics (McGreer et al. 2011) are more sensitive probes of the structure of reionization. Future work with additional GRB sightlines, in combination with numerical simulations, will enable systematic tests of the statistics of Ly $\alpha$  opacity (Gallerani et al. 2008) with a less-biased tracer of the end of reionization than quasars, which reside in more massive dark matter halos (Mesinger 2010).

#### 4. Ly $\alpha$ RED DAMPING WING ANALYSIS

We now analyze the red damping wing of Ly $\alpha$  to set constraints on the neutral hydrogen column density responsible for the absorption. We exclude the two regions shown in gray in the right panel of Figure 1, which include the foreground C IV absorber and the residuals from an unfortunately placed strong night sky line at 8919 Å. Because we do not detect any narrow lines from the host galaxy,  $z_{\text{GRB}}$  is a free parameter in all fits.

##### 4.1. Pure Host Absorption

Our first model assumes that all of the absorption is from a single absorber, presumably the host galaxy, at redshift  $z_{\text{GRB}}$ . This model is shown as the blue dashed line in Figure 1. Our best-fit parameters are  $\log(N_{\text{HI}}, \text{cm}^{-2}) = 18.62 \pm 0.18$  at  $z_{\text{GRB}} = 6.3269 \pm 0.0007$ . Only 5–10% of GRBs at  $z > 2$  have measured host hydrogen column densities this low (Chen et al. 2007; Fynbo et al. 2009).

Chen et al. (2007) argued that the distribution of  $\log(N_{\text{HI}})$  for a complete sample of GRBs offers a statistical sampling of sightlines from regions of massive-star formation and can be used to infer the escape fraction of ionizing photons in high- $z$  galaxies. In Figure 3, we show the distribution of available  $\log(N_{\text{HI}})$  measurements for  $z > 4$  GRBs (mostly compiled by Thöne et al. 2013). It is striking that the four highest-redshift GRBs include the three lowest values for  $\log(N_{\text{HI}})$  in the sample. Lower neutral hydrogen column densities imply a higher escape fraction. An Anderson-Darling k-sample test gives a probability of 1.8% that the distribution of column densities at  $z > 5.9$  comes from the same distribution as that at lower redshift. The redshift cut was not made blindly, so more data are needed to test whether the neutral hydrogen column distribution evolves to lower values at higher redshift. One concern is selection biases, particularly that sightlines with higher columns will potentially be associated with more dust extinction and thus less likely to have afterglows identified and spectra taken with adequate S/N, but it is not clear how much of a differential effect this could be between the  $z \approx 4$  and  $z \approx 6$  samples.

This result may be consistent with recent observations of a decreasing fraction of Ly $\alpha$ -emitters among Lyman-break galaxies at  $z > 6$ , which have also been modeled in terms of an increase in escape fraction (e.g., Dijkstra et al. 2014), although an increase in the neutral hydrogen fraction ( $\bar{x}_{\text{HI}}$ ) of the IGM (e.g., Schenker et al. 2012) is an alternative hypothesis. These are complementary observations, as GRBs are superior tracers of star formation at high redshift compared to flux-limited samples of galaxies (Tanvir et al. 2012).

Our non-detection of narrow absorption lines from the host galaxy may be simply a consequence of the low neutral hydrogen column density. Some of the strongest lines we expect in the limited wavelength interval of our continuum are Si II  $\lambda 1260$ , O I  $\lambda 1302$ , and C II  $\lambda 1334$ . We use the noise in the spectrum to estimate conservative  $3\sigma$  upper limits on the observed-frame EWs of these lines of 1 Å, 2.5 Å, and 2.5 Å, respectively. Assuming the optically-thin limit and the measured value of  $\log(N_{\text{HI}})$ , these correspond to upper limits on the gas-phase abundances of  $[Z/H] \lesssim -1.1$ ,  $-0.6$ , and  $-0.8$ , respectively (Asplund et al. 2009). If the IGM contributes to the neutral hydrogen column, these limits would have to be relaxed. Nevertheless, they are compatible with typical sub-solar abundance estimates for high- $z$  GRB host galaxies (e.g., Thöne et al. 2013; Chornock et al. 2013; Castro-Tirado et al. 2013) and we do not require unusually low abundances to explain the lack of detected absorption lines from the host.

##### 4.2. Pure IGM Absorption

Our second model ignores the likelihood of an absorber associated with the host galaxy and embeds a “naked” GRB in a uniform medium of constant  $\bar{x}_{\text{HI}}$ . We use the model of Miralda-Escude (1998) to approximate the effects of a partially neutral IGM. The model requires a lower redshift bound for neutral hydrogen absorption, which we fix to  $z = 6.0$  because it has no effect on the results, and an upper redshift bound that we assume is equal to  $z_{\text{GRB}}$ . The best fit is shown as the red dot-

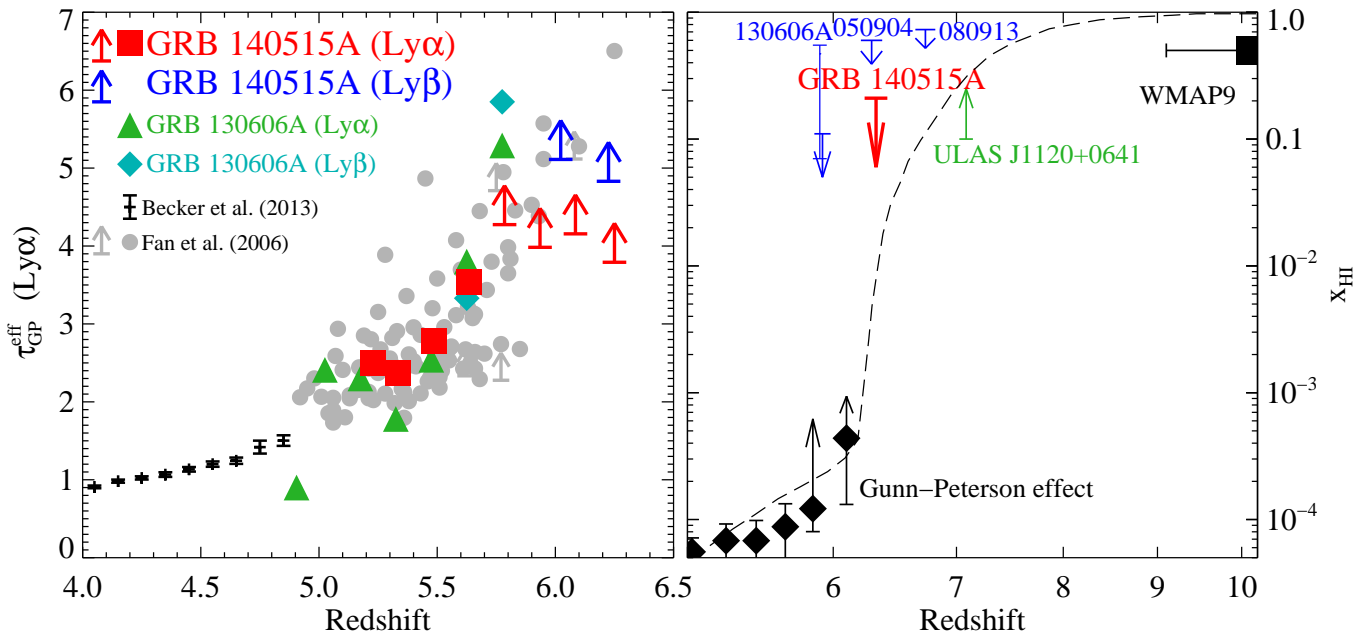


**Figure 2.** Redshift evolution of the IGM. *Left:* Ly $\alpha$  effective optical depth,  $\tau_{\text{GP}}^{\text{eff}}(\text{Ly}\alpha)$ , computed in bins of width  $\Delta z \approx 0.15$  in both Ly $\alpha$  and Ly $\beta$ , with arrows representing lower limits. The triangles and diamonds are the measurements from the sightline to GRB 130606A (Chornock et al. 2013). The comparison points were measured from Ly $\alpha$  absorption of quasars by Fan et al. (2006b) and Becker et al. (2013). *Right:* Neutral fraction of the IGM,  $\bar{x}_{\text{HI}}$ , showing the  $2\sigma$  limit from the hybrid IGM+host+bubble model for GRB 140515A in red and the other GRB constraints in blue (Chornock et al. 2013; Totani et al. 2006, 2014; Patel et al. 2010). The lower limit from observations of a  $z = 7.085$  quasar is in green (Mortlock et al. 2011; Bolton et al. 2011), along with measurements from quasar absorption (Fan et al. 2006b) and a step-function reionization fit to the microwave background polarization (Hinshaw et al. 2013). The dashed line is a fiducial late reionization model from Gnedin & Kaurov (2014).

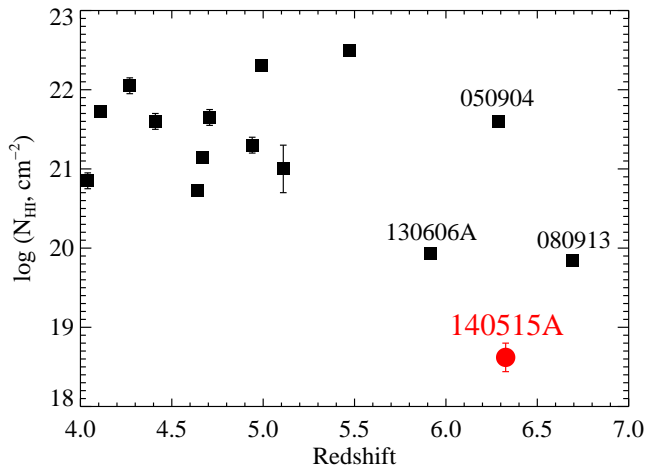


**Figure 3.** H I column density measurements for  $z > 4$  GRBs. Data from the literature were compiled by Thöne et al. (2013) and supplemented with a few more recent results (111008A: Sparre et al. 2014; 130606A: Chornock et al. 2013; Castro-Tirado et al. 2013; Totani et al. 2014; 140518A: Chornock et al. 2014b). GRBs at  $z \gtrsim 5.5$  appear to have lower hydrogen columns than those at lower redshift.

dashed line in Figure 1 and has  $z_{\text{GRB}} = 6.3282^{+0.0010}_{-0.0004}$  and  $\bar{x}_{\text{HI}} = 0.056^{+0.011}_{-0.027}$ . At the  $3\sigma$  level, the maximum value allowed for  $\bar{x}_{\text{HI}}$  is 0.09.

#### 4.3. Hybrid Model

The two models above represent possible extremes of absorption from only the host or IGM. If both are present, the situation is more complex. If we simply combine the models, the limits will relax and favor somewhat smaller values for  $\bar{x}_{\text{HI}}$  and  $\log(N_{\text{HI}})$  as the

two sources of opacity are both allowed to contribute. However, more properly treating the inhomogeneity of the IGM during of the end of reionization will considerably relax these constraints (Mesinger & Furlanetto 2008; McQuinn et al. 2008).

We address this issue by fitting a hybrid model with absorption from both the host and the IGM. This model has three free parameters ( $\log(N_{\text{HI}})$ ,  $\bar{x}_{\text{HI}}$ , and  $z_{\text{GRB}}$ ). We place the GRB in an ionized bubble and fix the radius of the bubble along our sightline to  $R_b = 10$  comoving Mpc. This choice is motivated by the simulations of McQuinn et al. (2008), who found H II regions of approximately this scale when  $\bar{x}_{\text{HI}}$  was globally equal to 0.5. The best-fit values are  $z_{\text{GRB}} = 6.3273$ ,  $\log(N_{\text{HI}}) = 18.43$ , and  $\bar{x}_{\text{HI}} = 0.12$ . The marginalized contours from our fit are shown in Figure 4. As expected, this significantly relaxes the constraint on  $\bar{x}_{\text{HI}}$ . Even with the favorable assumption about the existence of an ionized bubble,  $\bar{x}_{\text{HI}} < 0.21$  at the  $2\sigma$  level. We do not take into account the effect of inhomogeneity on the expected shape of the damping wing from the IGM (Mesinger & Furlanetto 2008). A larger bubble size would formally allow for even higher  $\bar{x}_{\text{HI}}$ , but such bubbles are rare unless  $\bar{x}_{\text{HI}}$  is low (McQuinn et al. 2008). Smaller ionized bubbles would only tighten this constraint.

The three fiducial models sample the range of variation of plausible reionization scenarios. All three models provide acceptable fits to the data, with reduced- $\chi^2$  values near 1.0, although the IGM-only model appears to be less adequate at the sharp edge of Ly $\alpha$ . The patchiness of the end of reionization will result in significant stochasticity along different sightlines (Mesinger & Furlanetto 2008; McQuinn et al. 2008) and a statistical ensemble of GRB

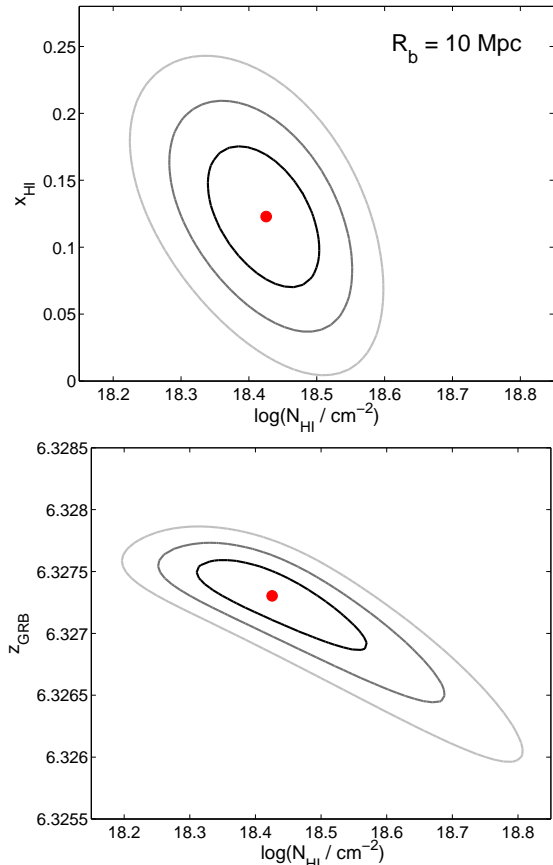


**Figure 4.** Contours (1, 2, and  $3\sigma$ ) from a three-parameter fit to the red damping wing of the Ly $\alpha$  profile. The GRB was assumed to lie at  $z_{\text{GRB}}$  in a host galaxy with a hydrogen column density  $\log(N_{\text{HI}})$ , residing in an ionized bubble of radius 10 comoving Mpc in a medium with an otherwise uniform neutral fraction  $\bar{x}_{\text{HI}}$ , which we constrain to be less than 0.21 at the  $2\sigma$  level.

sightlines will be necessary to measure cosmic variance and jointly constrain the models in more detail.

## 5. DISCUSSION AND CONCLUSIONS

We have presented an optical spectrum of the afterglow of GRB 140515A at  $z \approx 6.33$  and used it to provide constraints on the opacity and ionization state of the IGM.

This is now the fourth high- $z$  GRB for which a damping-wing analysis has been performed. Totani et al. (2006) found that for GRB 050904 at  $z=6.295$  (Kawai et al. 2006),  $\bar{x}_{\text{HI}} < 0.6$  at the 95% confidence level, but that the high host hydrogen column density inhibited tight constraints. McQuinn et al. (2008) examined the same spectrum and argued that proper treatment of inhomogeneity will relax the constraint even further. Patel et al. (2010) were unable to place meaningful constraints on the sightline to the  $z=6.733$  GRB 080913 due to the low S/N of the data, but quoted  $\bar{x}_{\text{HI}} < 0.73$  at the 90% confidence level. The high- $z$  GRB afterglow with the highest S/N observations was GRB 130606A at  $z=5.913$ . Chornock et al. (2013) set a  $2\sigma$  upper limit of  $\bar{x}_{\text{HI}} < 0.11$  for a model with IGM absorption extending up to  $z_{\text{GRB}}$ . Totani et al. (2014) argued that their spectra of the same burst disfavored a pure host-galaxy absorption model. If they allowed IGM absorption at redshifts up to  $z_{\text{GRB}}$ , they found  $\bar{x}_{\text{HI}} = 0.086^{+0.012}_{-0.011}$ . Lowering the

upper redshift to  $z=5.83$  allowed values for  $\bar{x}_{\text{HI}}$  up to  $\sim 0.5$ . However, their claims are based on a subtle 0.6% deviation from the pure host-galaxy model.

Quasars are the other major observational probe of the ionization state of the IGM at these redshifts, but variations in intrinsic properties and difficulties in modeling quasar near zones make the interpretation more controversial (e.g., Mesinger & Haiman 2007; Carilli et al. 2010). The highest-redshift quasar currently known, ULAS J1120+0641 at  $z=7.085$ , exhibits a red damping wing ascribed to  $\bar{x}_{\text{HI}} > 0.1$  (Mortlock et al. 2011), although the exact value depends on the unknown details of the quasar’s lifetime (Bolton et al. 2011).

In our toy model with an  $R_b=10$  Mpc (comoving) bubble, we set a  $2\sigma$  upper limit of  $\bar{x}_{\text{HI}} < 0.21$ , with a best-fit value of  $\bar{x}_{\text{HI}} = 0.12$ . Models with smaller or nonexistent H II regions will prefer even smaller values for  $\bar{x}_{\text{HI}}$ . The sharp decrement in flux at Ly $\alpha$  is incompatible with a large neutral fraction in the IGM at  $z \approx 6.3$  in almost any model. We compare this value to the others described above in the righthand panel of Figure 2. The GRB constraints on  $\bar{x}_{\text{HI}}$  are still above predictions from models of the IGM tuned to reproduce the Ly $\alpha$  forest at  $z \lesssim 6$  (e.g., Gnedin & Kaurov 2014).

The reasonable quality of the constraint on  $\bar{x}_{\text{HI}}$  from these data despite the short integration time is a result of the brightness of the afterglow and the low hydrogen column density of the host. A future sample of GRBs at even higher redshift, if it can be collected, would serve as an excellent record of the end of reionization.

We thank the Gemini staff, particularly Lucas Fuhrman, for their superb assistance in obtaining these observations. The Berger GRB group at Harvard is supported by the National Science Foundation under Grant AST-1107973. Based in part on observations obtained under Program ID GN-2014A-Q-38 (PI: Berger) at the Gemini Observatory, which is operated by the Association of Universities for Research in Astronomy, Inc., under a cooperative agreement with the NSF on behalf of the Gemini partnership: the National Science Foundation (United States), the Science and Technology Facilities Council (United Kingdom), the National Research Council (Canada), CONICYT (Chile), the Australian Research Council (Australia), Ministério da Ciência, Tecnologia e Inovação (Brazil) and Ministerio de Ciencia, Tecnología e Innovación Productiva (Argentina).

*Facilities:* Gemini:Gillett (GMOS-N)

## REFERENCES

- Asplund, M., Grevesse, N., Sauval, A. J., & Scott, P. 2009, *ARA&A*, 47, 481
- Barkana, R., & Loeb, A. 2004, *ApJ*, 601, 64
- Becker, G. D., Hewett, P. C., Worseck, G., & Prochaska, J. X. 2013, *MNRAS*, 430, 2067
- Bolton, J. S., Haehnelt, M. G., Warren, S. J., et al. 2011, *MNRAS*, 416, L70
- Carilli, C. L., Wang, R., Fan, X., et al. 2010, *ApJ*, 714, 834
- Castro-Tirado, A. J., Sánchez-Ramírez, R., Ellison, S. L., et al. 2013, arXiv:1312.5631
- Chen, H.-W., Prochaska, J. X., & Gnedin, N. Y. 2007, *ApJ*, 667, L125
- Chornock, R., Berger, E., Fox, D. B., et al. 2013, *ApJ*, 774, 26
- Chornock, R., Fox, D. B., & Berger, E. 2014a, *GRB Coordinates Network*, 16269, 1

- Chornock, R., Fox, D. B., Cucchiara, A., Perley, D. A., & Levan, A. 2014b, GRB Coordinates Network, 16301, 1
- Cucchiara, A., Levan, A. J., Fox, D. B., et al. 2011, *ApJ*, 736, 7
- D’Avanzo, P., et al. 2014, GRB Coordinates Network, 16267, 1
- Dijkstra, M., Wyithe, S., Haiman, Z., Mesinger, A., & Pentericci, L. 2014, *MNRAS*, 440, 3309
- Fan, X., Carilli, C. L., & Keating, B. 2006a, *ARA&A*, 44, 415
- Fan, X., Strauss, M. A., Becker, R. H., et al. 2006b, *AJ*, 132, 117
- Fong, W., Chornock, R., Fox, D., & Berger, E. 2014, GRB Coordinates Network, 16274, 1
- Fynbo, J. P. U., Jakobsson, P., Prochaska, J. X., et al. 2009, *ApJS*, 185, 526
- Gallerani, S., Salvaterra, R., Ferrara, A., & Choudhury, T. R. 2008, *MNRAS*, 388, L84
- Gnedin, N. Y., & Kaurov, A. A. 2014, arXiv:1403.4251
- Greiner, J., Krühler, T., Fynbo, J. P. U., et al. 2009, *ApJ*, 693, 1610
- Hinshaw, G., Larson, D., Komatsu, E., et al. 2013, *ApJS*, 208, 19
- Hook, I. M., Jørgensen, I., Allington-Smith, J. R., et al. 2004, *PASP*, 116, 425
- Kawai, N., Kosugi, G., Aoki, K., et al. 2006, *Nature*, 440, 184
- Lamb, D. Q., & Reichart, D. E. 2000, *ApJ*, 536, 1
- McGreer, I. D., Mesinger, A., & Fan, X. 2011, *MNRAS*, 415, 3237
- McQuinn, M., Lidz, A., Zaldarriaga, M., Hernquist, L., & Dutta, S. 2008, *MNRAS*, 388, 1101
- Mesinger, A. 2010, *MNRAS*, 407, 1328
- Mesinger, A., & Furlanetto, S. R. 2008, *MNRAS*, 385, 1348
- Mesinger, A., & Haiman, Z. 2007, *ApJ*, 660, 923
- Miralda-Escude, J. 1998, *ApJ*, 501, 15
- Mortlock, D. J., Warren, S. J., Venemans, B. P., et al. 2011, *Nature*, 474, 616
- Patel, M., Warren, S. J., Mortlock, D. J., & Fynbo, J. P. U. 2010, *A&A*, 512, L3
- Salvaterra, R., Della Valle, M., Campana, S., et al. 2009, *Nature*, 461, 1258
- Schenker, M. A., Stark, D. P., Ellis, R. S., et al. 2012, *ApJ*, 744, 179
- Schlafly, E. F., & Finkbeiner, D. P. 2011, *ApJ*, 737, 103
- Songaila, A., & Cowie, L. L. 2002, *AJ*, 123, 2183
- Sparre, M., Hartoog, O. E., Krühler, T., et al. 2014, *ApJ*, 785, 150
- Tanvir, N. R., Fox, D. B., Levan, A. J., et al. 2009, *Nature*, 461, 1254
- Tanvir, N. R., Levan, A. J., Fruchter, A. S., et al. 2012, *ApJ*, 754, 46
- Thöne, C. C., Fynbo, J. P. U., Goldoni, P., et al. 2013, *MNRAS*, 428, 3590
- Totani, T., Kawai, N., Kosugi, G., et al. 2006, *PASJ*, 58, 485
- Totani, T., Aoki, K., Hattori, T., et al. 2014, *PASJ*, accepted, arXiv:1312.3934
- van Dokkum, P. G. 2001, *PASP*, 113, 1420